Output feedback assistive control of single-DOF SEA powered exoskeletons

Iman Kardan and Alireza Akbarzadeh
Center of Excellence on Soft Computing and Intelligent Information Processing, Mechanical Engineering Department, Ferdowsi University of Mashhad, Mashhad, Iran

Abstract

Purpose – This paper aims to overcome some of the practical difficulties in assistive control of exoskeletons by developing a new assistive algorithm, called output feedback assistive control (OFAC) method. This method does not require feedbacks from force, electromyography (EMG) or acceleration signals or even their estimated values.

Design/methodology/approach – The presented controller uses feedbacks from position and velocity of the output link of series elastic actuators (SEAs) to increase the apparent integral admittance of the assisted systems. Optimal controller coefficients are obtained by maximizing the assistance ratio subjected to constraints of stability, coupled stability and a newly defined comfort measure.

Findings – The results confirm the effectiveness of using the inherent properties of SEAs for removing the need for extra controversial sensors in assistive control of 1 degree of freedom (1-DOF) SEA powered exoskeletons. The results also clearly indicate the successful performance of the OFAC method in reducing the external forces required for moving the assisted systems.

Practical implications – As the provided experiments indicate, the proposed method can be easily applied to single DOF compliantly actuated exoskeletons to provide a more reliable assistance with lower costs. This is achieved by removing the need for extra controversial sensors.

Originality/value – This paper proposes a novel assistive controller for SEA-powered exoskeletons with a simple model-free structure and independent of any information about interaction forces and future paths of the system. It also removes the requirement for the extra sensors and transforms the assistive control of the compliantly actuated systems into a simpler problem of position control of the SEA motor.

Keywords Exoskeletons, Rehabilitation robots, Compliant mechanisms, Integral admittance shaping, Output feedback assistive control, Series elastic actuators

Paper type Research paper

1. Introduction

Following the first attempts in General Electric Co. (Mosher, 1967; Bogue, 2009) and Mihajlo Pupin Institute (Vukobratovic, 2007), researches for developing exoskeleton robots found a growing interest. In recent years, some successful instances of these robots are manufactured and even commercialized. BLEEX (Kazerooni and Steger, 2006; Kazerooni *et al.*, 2006), HULC (Kopp, 2011), HAL (Kawamoto and Sankai, 2002; Sankai, 2010), ReWalk (Esquenazi *et al.*, 2012), RoboKnee (Pratt *et al.*, 2004) and LOPES (Veneman *et al.*, 2007; Vallery *et al.*, 2008) are some of the better known exoskeletons.

Yan *et al.* (2015) presented a comprehensive review on control strategies of exoskeletons. They classified exoskeletons in three main categories. The first category includes load-carrying exoskeletons. The second category of the exoskeletons, focus on rehabilitation of patients in executing some predefined motions such as walking and sit to stand cycles. The third category of exoskeletons are used in rehabilitation of patients with muscle weakness or joint disease through reducing the loads on wearer's muscles and joints and providing some assisting forces. Elderlies and osteoarthritis patients are the main users of these robots. However, by reducing the muscles loads and providing the assisting forces, these robots can also be used for power augmentation of healthy subjects.

Diverse algorithms are designed for the third category of exoskeleton robots. These algorithms are termed as "assistive controllers" because they assist wearers in different tasks by providing some portion of required muscles or joints forces. Some of these methods provide assistive forces according to the muscles or joints efforts, measured through electromyography (EMG) sensors, as in HAL-3 (Lee and Sankai, 2002a, 2002b) and (Rosen *et al.*, 2001; Cheng *et al.*, 2003), or estimated through ground reaction force sensors, as in RoboKnee (Pratt *et al.*, 2004). Some other methods aim at reducing the apparent impedance of the user's limbs by using a combination of EMG and force sensors (Kiguchi *et al.*, 2001; Kiguchi *et al.*, 2004; Morbi *et al.*, 2014). Active and adaptive impedance control (Aguirre-Ollinger *et al.*, 2007; Hussain *et al.*, 2013), inertia compensation (Aguirre-Ollinger *et al.*, 2011, 2012) and integral admittance (IA) shaping (Nagarajan *et al.*, 2016) are other algorithms designed for reducing the apparent impedance of the user's limbs. Adaptive oscillators-based methods (Ronsse *et al.*,

The current issue and full text archive of this journal is available on Emerald Insight at: **www.emeraldinsight.com/0143-991X.htm**

Industrial Robot: An International Journal
44/3 (2017) 275–287

[DOI 10.1108/IR-08-2016-0214]

Received 14 June 2016
Revised 4 October 2016
Accepted 5 October 2016

2011) and user's intent estimation algorithms (Karavas *et al.*, 2015) are also used in assistive control of exoskeletons.

However, these methods need feedbacks from muscles, joints or contact forces as well as the robot accelerations or the user's intended motion. Therefore, the use of extra sensors such as load cells, accelerometers or EMG sensors is indispensable. The well-known problems of these sensors may limit the application of the available methods. Immaturity of EMG sensors, besides relatively heavy signal processing and task and time dependency of EMG signals, are the main barriers for practical application of these devices (Yan *et al.*, 2015). Force and acceleration sensors suffer from being noise contaminated and leading to instability in the case of impact contacts (Pratt *et al.*, 2002). The stability issue gains more importance for exoskeleton robots where impact contacts are inevitable. Some references use estimated force values for implementation of assistive algorithms (Uemura *et al.*, 2006; Unluhisarcikli *et al.*, 2011). Yet, a good estimation of forces requires persistently exciting input signals and a reliable model of system dynamics which impede practical application of these algorithms.

Advantages of SEAs over stiff actuators such as low and adjustable output impedance, low friction, impact resistance, increased efficiency due to energy storage and increased stability are well studied by Vanderborght *et al.* (2013) and Cestari *et al.* (2014). The present paper will consider the possibility of using inherent properties of series elastic actuators (SEAs) for overcoming present difficulties in assistive control of exoskeletons. As shown in Figure 1, a linear series elastic actuator, called FUM-LSEA, is manufactured by the FUM Robotics Lab at the Ferdowsi University of Mashhad (Kamali *et al.*, 2016). The FUM-LSEA is used in the present work for performing the experiments.

Considering the existing body of the literature and the previous discussions, finding a way of reducing apparent impedance of wearer's limbs without using force, EMG or acceleration signals or even their estimated values as well as wearer's intended motion, will play an important role in development of assistive exoskeleton robots. Using the inherent characteristics of the SEAs, this paper presents a novel assistive controller for compliantly actuated exoskeletons. The proposed control algorithm uses feedback signals from position and velocity of the output link of SEAs to reduce apparent impedance of the connected systems. The presented method satisfies all the desired discussed features and called output feedback assistive control (OFAC).

The rest of the paper is organized as follows. The proposed OFAC method is introduced in Section 2. Section 3 gives stability and coupled stability conditions for the OFAC method.

Figure 1 FUM-LSEA

Section 4 formulates a constrained optimization problem for finding optimal controller coefficients. Simulation results are presented in Section 5 to demonstrate the performance of the OFAC method. Section 6 provides some experimental results to verify the practical performance of the OFAC method. Finally, Section 7 concludes the paper.

2. Output feedback assistive control

Generally, each 1 degree of freedom (1-DOF) physical system, moving near its equilibrium point, can be linearized as a mass-spring-damper system as shown in Figure 2. The linear 1-DOF mass-spring-damper system is widely used in teleoperation and haptic studies for modeling the physical or virtual environments. This model is even used as a representation of the human operators (Amini *et al.*, 2015; Fite *et al.*, 2004; Lee and Spong, 2006; Sirouspour and Shahdi, 2006; Lawrence and Chapel, 1994; Vander Poorten *et al.*, 2006; Focchi *et al.*, 2016).

In this model, F_h is an external force applied to the system and M_h, B_h and K_h denote inertia, damping and stiffness of the dynamical system, respectively. It is noteworthy that, moreover to the elastic elements of the system, the stiffness coefficient may represent a linearized model of gravity induced torque in a rotational system. The well-known equation of motion of the system in Figure 2 is given by equation (1):

$$F_h = M_h\ddot{x}_h + B_h\dot{x}_h + K_h x_h \tag{1}$$

Coupling the system to a linear SEA as a supplementary force source, the overall structure of the SEA powered system is shown in Figure 3. In Figure 3, F_m is the actuating force provided by the SEA motor and the variables M_m, B_m and K_m define impedance coefficients of the equivalent linear model of the SEA input section containing motor, belt, pulleys, ball screw, nut and moving block. Note that integral causality is met for both of the bond-graph models in Figures 2 and 3.

It is easy to derive the equations of motion of the compliantly actuated system of Figure 3 as given in equation (2):

$$\begin{cases} F_h = M_h\ddot{x}_h + B_h\dot{x}_h + K_h x_h + K_s(x_h - x_m) \\ \qquad + B_s(\dot{x}_h - \dot{x}_m) \\ F_m = M_m\ddot{x}_m + B_m\dot{x}_m + K_m x_m - K_s\,(x_h - x_m) \\ \qquad - B_s(\dot{x}_h - \dot{x}_m) \end{cases} \tag{2}$$

The design objective of the assistive controller can now be better defined. The SEA should be controlled such that the

Figure 2 Representation of a linearized 1-DOF system

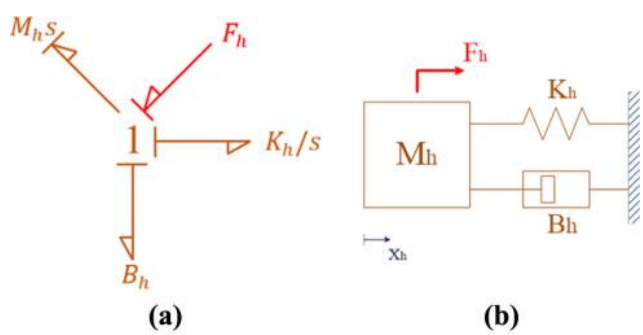

Notes: (a) Bond-graph; (b) block diagram

Figure 3 Linearized model of a 1-DOF system coupled to a SEA

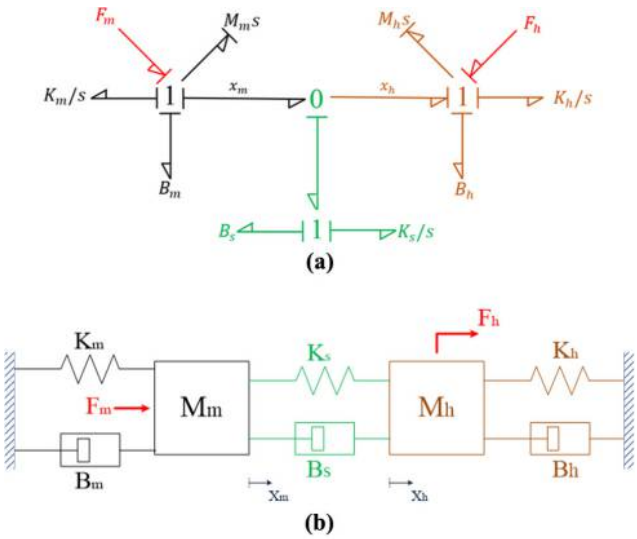

Notes: (a) Bond-graph; (b) block diagram

required external force for moving the mass M_h of the coupled system of equation (2) in an arbitrary path, is less than that of the isolated system of equation (1). This objective is termed as torque reduction by Nagarajan *et al.* (2016). Another design objective may be defined as increasing the amplitude of motion of the coupled system of equation (2) over the isolated system of equation (1) for an identical external force. This objective is termed as motion amplification by Nagarajan *et al.* (2016). It is clear that both of these objectives are equivalent to increasing apparent admittance of the system.

To study the effect of the controller in low frequencies, specifically to consider DC gain of the system, it is better to work with integral impedance, $\hat{Z}(s)$, and IA, $\hat{Y}(s)$, of the system rather than the regular definition of impedance, $Z(s)$, and admittance, $Y(s)$ (Nagarajan *et al.*, 2016).

Laplace transform can be applied to derive the IA of the isolated system of equation (1) as given in equation (3). Note that, here the IA of the system is identical to its transfer function:

$$\hat{Y}(s) = G(s) = \frac{x_h}{F_h} = \frac{1}{M_h S^2 + B_h S + K_h} \tag{3}$$

Nagarajan *et al.* (2016) have proposed a unified approach for assistive control of exoskeletons. They considered a soft coupling between exoskeleton and human body and presented an algorithm to shape the apparent IA of the user's limb for his/her muscles.

To assess the assisting degree of their proposed algorithm, Nagarajan *et al.* (2016) defined two terms of assistance ratio, $\mathcal{A}(\omega_f)$, and resistance ratio $\mathcal{R}(\omega_f)$ as:

$$\begin{cases} \mathcal{A}(\omega_f) = \dfrac{1}{\omega_f}\displaystyle\int_0^{\omega_f} \max\left(\frac{|\hat{Y}_t(j\omega)| - |\hat{Y}(j\omega)|}{|\hat{Y}(j\omega)|}, 0\right) d\omega \\ \mathcal{R}(\omega_f) = \dfrac{1}{\omega_f}\displaystyle\int_0^{\omega_f} \min\left(\frac{|\hat{Y}(j\omega)| - |\hat{Y}_t(j\omega)|}{|\hat{Y}(j\omega)|}, 0\right) d\omega \end{cases} \tag{4}$$

where $\hat{Y}_t$ is IA of the assisted system and ω_f is the upper bound of the frequency interval $[0 \ \ \omega_f]$ over which the assistance should be made. Next, they defined a cost function for maximizing the assistance ratio and minimizing the resistance ratio over the predefined frequency interval subject to constraints of stability and coupled stability. They also added the constraint of equation (5) to maintain the damping ratio of the assisted system, ξ_t, close enough to that of the unassisted system, ξ, as a measure of comfort. Here, ε defines the allowed variation in the damping ratio:

$$\frac{|\xi_t - \xi|}{\xi} \le \varepsilon \tag{5}$$

This work (Nagarajan *et al.*, 2016) presents a good assistive control algorithm due to its simplicity and the low number of required sensors. However, Nagarajan *et al.* (2016) showed that their proposed method requires filtered feedback from exoskeleton accelerations for a complete shaping of the IA. Therefore, despite of being an effective assistive technique, it suffers from the well-known problems of noisy accelerometers.

In this paper, we use the concept of shaping the apparent IA of the assisted system and propose a novel OFAC algorithm, OFAC. This method uses a feedback from SEA output to give a desired shape to the apparent IA of the assisted system. The proposed OFAC method adjusts desired position of the SEA motor, x_{md}, according to control law of equation (6):

$$x_{md} = \alpha x_h + \beta \dot{x}_h \tag{6}$$

Supposing that the SEA motor is an ideal position source, its position, x_m, will immediately reach the desired value. In other words, $x_m = x_{md}$. Considering the first row of equation (2), in this case equation (7) defines the equation of motion of the assisted system and Figure 4 depicts its block diagram:

$$\begin{cases} F_h + F_s = M_h \ddot{x}_h + B_h \dot{x}_h + K_h x_h \\ F_s = B_s(\dot{x}_m - \dot{x}_h) + K_s(x_m - x_h) \end{cases} \tag{7}$$

According to Figure 4, the relation between F_h and x_h can be calculated as equation (8) in which M_t, B_t and K_t are coefficients of the apparent impedance of the assisted system as seen by the external force:

$$\begin{aligned} &\hat{Y}_t(s) = G_t = \frac{x_h}{F_h} = \frac{1}{M_t s^2 + B_t s + K_t} \\ &\begin{cases} M_t = M_h - \beta B_s \\ B_t = B_h - \beta K_s - (\alpha - 1) B_s \\ K_t = K_h - K_s(\alpha - 1) \end{cases} \end{aligned} \tag{8}$$

Figure 4 Block diagram of the assisted system, supposing the SEA motor as an ideal position source

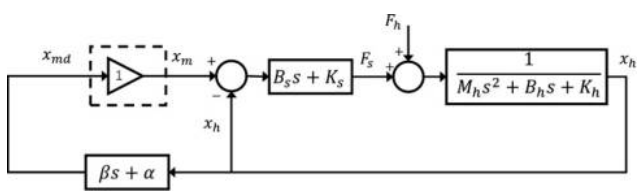

Industrial Robot: An International Journal
Volume 44 · Number 3 · 2017 · 275–287

Note that the SEA is supposed to ideally follow the desired positions produced by the OFAC algorithm of equation (6). Actually, it is assumed that the SEA position control loop has a bandwidth sufficiently higher than the maximum frequency of possible motions of the assisted system. This seems to be a reasonable assumption for the target systems of this paper, i.e. exoskeleton robots which operate at the frequencies of human motions.

To assure assisting over the entire frequency interval, we define the point assistance ratio as:

$$\mathcal{PA}(\omega) = \frac{|\hat{Y}_t(j\omega)| - |\hat{Y}(j\omega)|}{|\hat{Y}(j\omega)|}. \tag{9}$$

This definition guarantees that assistance is accomplished for each frequency of $\omega \in [0 \quad \omega_f]$ as long as the condition of equation (10) is met:

$$\mathcal{PA}(\omega) \geq 0 \quad \forall \omega \in [0 \quad \omega_f] \tag{10}$$

Moreover, instead of using the damping ratio as the measure of comfort, we consider the phase similarity between IAs of the assisted and unassisted system as given in equation (11). Here, φ_t and φ denote the phase angles of the IAs of the assisted and the unassisted systems, respectively, and δ defines the maximum allowable phase difference:

$$\left|\frac{\varphi_t(\omega) - \varphi(\omega)}{\varphi(\omega)}\right| \leq \delta \quad \forall \omega \in [0 \quad \omega_f] \tag{11}$$

The authors believe that this definition gives a better comfort measure because it will be more comfortable for the user if the assisted motion requires a torque trajectory having a phase angle similar to that of the unassisted motion. However, there is no widely accepted definition of the user's comfort (Tang and Cao, 2012).

The proposed controller has a very simple structure and conforms to the design constraints of being independent of any information about interaction forces and future path of the system. It also removes the requirement for the controversial sensors and transforms the assistive control of the SEA-powered systems into the simple problem of position control of the SEA motor. Moreover, this algorithm has a model-free structure and does not explicitly include dynamic equations of the system.

In addition to conditions of equations (10) and (11), there are other theoretical and practical constraints which restrict the permissible region of selecting control parameters. Stability of the assisted system and its coupled stability in connection with external environments are two of the most important limiting factors. The assisted system should be stable and should remain stable while interacting with external environments.

3. Stability analysis

Considering the transfer function of equation (8), stability conditions of the assisted system can be easily obtained as the upper limits of the α and β coefficients as:

$$\begin{cases} K_t \geq 0 \Rightarrow \alpha \leq 1 + \dfrac{K_h}{K_s} \\ B_t \geq 0 \Rightarrow \beta \leq \dfrac{B_h - B_s(\alpha - 1)}{K_s} \\ M_t \geq 0 \Rightarrow \beta \leq \dfrac{M_h}{B_s} \end{cases} \Rightarrow \begin{cases} \alpha \leq 1 + \dfrac{K_h}{K_s} \\ \beta \leq min\left\{\dfrac{B_h - B_s(\alpha - 1)}{K_s}, \dfrac{M_h}{B_s}\right\} \end{cases} \tag{12}$$

For the systems that come into contact with external environments, coupled stability of the system and environment should also be assessed. It is shown by Colgate (1988) that LTI plants interacting with a passive environment at a single port will have the coupled stability property if and only if they remain stable when coupled to the "worst environments". Such environments are lossless and are composed of a single spring or a single mass. They exactly add $\pm 90°$ phase lag which is the most possible phase lag that can be added by a passive environment.

Coupling to a mass or a spring is simply equivalent to adding some values to mass or stiffness of the assisted system. The added values are positive because negative masses or negative spring constants will not occur in real-world physical environments. According to equation (12), the increased mass or stiffness of the assisted system will only give a rise to the upper limits of the α and β coefficients, i.e. spreading their permissible range. Hence, assuring stability of the assisted system will guarantee its coupled stability as well. In the other words, equation (12) gives necessary and sufficient conditions for simultaneously assuring stability and coupled stability of the assisted system.

The passivity concept is a common method of stability analysis and controller design in a wide array of applications, specifically in teleoperation systems (Vander Poorten *et al.*, 2006; Focchi *et al.*, 2016; Lawrence, 1993; Ryu *et al.*, 2004; Hogan, 1989; Niemeyer and Slotine, 1991; Haddadi and Hashtrudi-Zaad, 2010; Haddadi *et al.*, 2015).

The passivity-based controllers are said to be conservative, as they guarantee the coupled stability of the controlled systems, regardless of the environment type. The only constraint is that both of the closed loop system and the environment should be passive. Therefore, the passivity constraint adds some robustness to the closed loop system against the variations in the environment parameters.

4. Parameter selection for maximum assistance

Optimal control parameters are chosen by solving constrained optimization problem of maximizing the assistance ratio [equation (4)], or equivalently minimizing its reciprocal, while maintaining the constraints of point assistance [equation (10)], comfort [equation (11)], stability and coupled stability [equation (12)]. The constrained optimization problem is formulated in equation (13):

$$\underset{\alpha,\ \beta}{\text{minimize}} \quad \frac{1}{\mathcal{A}(\omega_f)}$$
subject to: equation. 10, equation. 11 & equation. 12. (13)

Among diverse algorithms developed for constrained optimization problems, in this paper, interior-point algorithm is selected and applied by using fmincon command from MATLAB optimization toolbox. This algorithm needs only function evaluation and not its gradient which is hard to obtain in our case.

5. Simulation

In this section, performance of the proposed OFAC method is compared with the IA shaping algorithm presented by Nagarajan *et al.* (2016). Table I shows assumed values for the system parameters which are obtained from (Nagarajan *et al.*, 2016) where the parameters are given for a rotary system. The rotary units of the values are dropped and linear units are assigned.

Solving the constrained optimization problem of equation (13), maximum assistance ratio of $\mathcal{A}(\omega_f) = 0.15$ is achieved by applying the OFAC method and optimal control parameters are obtained as $\alpha = 1.0015$ and $\beta = 0.0012$. Beside the optimization method, a global search is also performed to visualize the permissible region of selecting the control parameters and their optimal values as depicted in Figure 5.

As noted in Nagarajan *et al.* (2016), by applying the IA shaping algorithm, maximum achievable assistance ratio of $\mathcal{A}(\omega_f) = 0.14$ is reported for the same values of the system parameters except for the comfort measure which is defined in a different way. However, they did not report ε value for their simulations.

Figure 6(a) and (c), respectively, compare the magnitude and phase diagrams of the IA of the unassisted system with those of the system optimally assisted by the two methods of the OFAC and the IA shaping. Point assistance ratio profiles, $\mathcal{PA}(\omega)$, for optimal control parameters of the two methods are also compared in Figure 6(b).

According to Figure 6(b), although the IA shaping algorithm provides more assistance in the lower frequencies, the OFAC method clearly outperforms it in the higher frequencies. The superior performance of the OFAC method is specifically more evident near the damped natural frequency of the unassisted system, $\omega_d = 3.98\ [rad/s]$. Figure 6(c) indicates that the OFAC method also has a great phase shifting performance near the damped natural frequency of the unassisted system. Regarding the fact that during lots of normal tasks, like normal walking, human limbs are moved at their natural frequencies to minimize energy consumption (Kuo, 2001), this could be a great achievement for the OFAC method to provide maximum assistance with minimum phase shifting in the natural frequency of systems especially in the case of exoskeletons.

Further assessment of the OFAC method is performed by applying harmonic paths to the unassisted and optimally assisted systems and comparing the required force trajectories for moving the systems in these paths. Figure 7 illustrates the required force trajectories. The first path, named as Path I, has a frequency of 2 $[rad/s]$ and an amplitude of 1 $[m]$. The second

Table I System parameters used in the simulation

Parameter	Value
M_h [kg]	3.38
B_h [Ns/m]	3.50
K_h [N/m]	54.70
ω_f [rad/s]	10
M_m [kg]	0.01178
B_m [Ns/m]	0.345
K_m [N/m]	0.339
δ [−]	0.65
B_s [Ns/m]	9.47
K_s [N/m]	1,905

Figure 5 Permissible region of selecting the control parameters

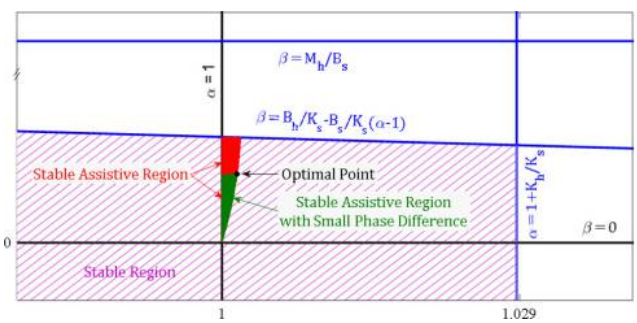

Figure 6 Performance of the OFAC method in comparison with the IA shaping algorithm

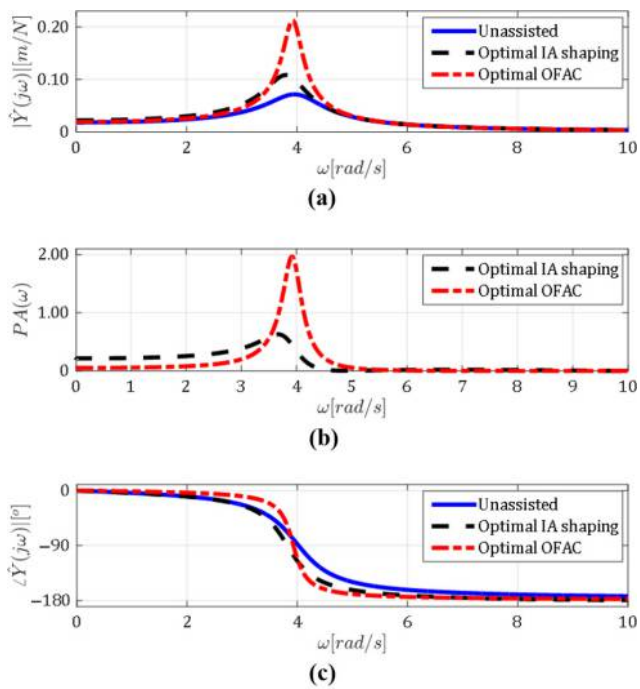

Notes: (a) Magnitude diagram; (b) point assistance profile; (c) phase diagram

Figure 7 Simulation of the OFAC method in two sample paths

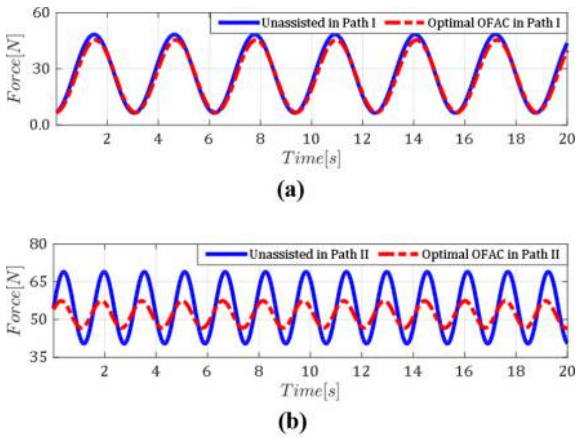

Notes: (a) Required force in Path I; (b) required force in Path II

path, named as Path II, has a frequency of 4 [*rad/s*] and an amplitude of 2 [*m*].

The results clearly indicate that the proposed OFAC method effectively reduces the required forces for moving the assisted system, especially when the system moves in frequencies close to its damped natural frequency. Superiority of the proposed OFAC method is better appreciated by recalling the fact that these results are obtained by using only two feedbacks from output position and velocity, rather than position, velocity and acceleration feedbacks in the IA shaping algorithm (Nagarajan *et al.*, 2016). This reduces the number of required sensors and eliminates the aforementioned problems with accelerometers. Moreover, OFAC method has only two controller gains, rather than four adjustable parameters in the IA shaping method. This makes the gain tuning process of the OFAC method much easier.

Regarding Figure 5, the selected point of optimal controller coefficients is considerably far from the stability margins. This somehow indicates the robustness of the optimally assisted system against the variations in the system parameters. Relatively large changes in the system parameters can occur while the assisted system maintains its stability. In this case, fixing all other system and controller parameters, the system stiffness can be reduced to $K_h = 2.9$ [N/m], the system damping coefficient can be decreased to $B_h = 2.3$ [Ns/m] and the system mass can be lowered to $M_h = 0.012$ [kg] before the occurrence of instability. This corresponds to 95 per cent per cent reduction in K_h, 34 per cent reduction in B_h and 99 per cent per cent reduction in M_h. Note that these results are obtained by fixing the controller coefficient at $\alpha = 1.0015$ and $\beta = 0.0012$ and changing only one system parameter each time. Therefore, it is observed that, in this case, the OFAC controller provides a great stability robustness. However, the performance of the controller, i.e. the assistance ratio is also affected by the changes in the system parameters. Large variations in the system parameters can degrade the performance of the controller. Note that this discussion only provides a rule of thumb in robustness analysis of the OFAC method. The addition of the stability and performance robustness conditions to the constraints of the controller coefficient optimization and studying the effect of simultaneous changes in the system parameters, need a deeper study which will be considered in future works.

6. Experimental evaluation

In this section, the practicality of the proposed OFAC method is evaluated by running some experiments. A 1-DOF lower limb exoskeleton, FUM-Physio, is chosen as the test bed for performing the experiments.

6.1 FUM-Physio as a single-DOF lower limb exoskeleton

As shown in Figure 8, FUM-Physio is a single link robot designed for automated knee therapy. Two separate mechanisms are considered to adjust the motor height and the fore-aft position of the seat. These mechanisms provide the robot with the capability of adapting to different patients of diverse heights by coinciding the axes of rotation of the patients' knee and the robot arm. The FUM-Physio is also equipped with a monitor that motivates the patients to follow the physiotherapist orders by playing simple interactive games. According to the physiotherapy plan, the robot may be controlled to assist or resist the patient's motions or to perform different isometric, isotonic and isokinetic exercises and so on.

Primary actuation of the robot is performed through the position mode of a 1 [kW] AC servo motor, by Delta Co., and the required torque is measured through CN5 analog monitor output of the motor drive. However, the FUM-Physio is designed in a way that the FUM-LSEA can be easily installed between the base and the robot arm as a supplementary power source as shown in Figure 9.

Besides the exoskeleton applications, reducing the required forces for moving the body limbs will also be effective in assistive physiotherapy exercises. In these exercises, the physiotherapist assists the patients' limbs in performing specific movements. This helps the patients to extend the motion ranges of their injured limbs and expedites the recovery

Figure 8 FUM-Physio

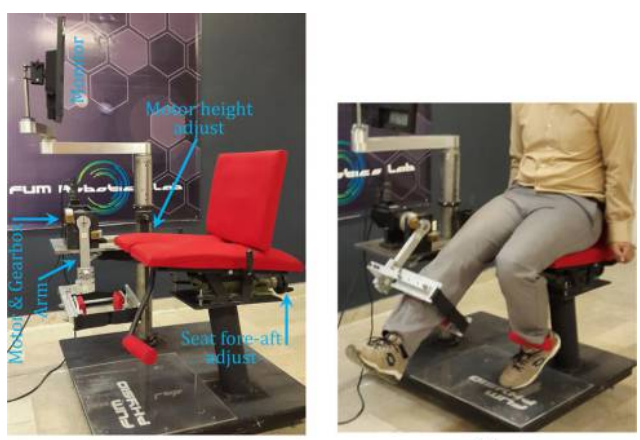

Notes: (a) Overview of the robot; (b) robot and the user

Figure 9 Installation of FUM-LSEA on FUM-Physio

process. Automating the assistive exercises, the amount of the assistance provided to the patients can be set exactly or can be adjusted adaptive to the patients' progress. Applying the OFAC method, the controller coefficients can be adjusted to provide the desired amount of assistance. The patients feel lighter limbs and move them easier which in turn leads to an extended range of motions.

6.2 Modeling

While the FUM-LSEA is uninstalled, the FUM-Physio resembles a physical pendulum whose well-known linearized equation of motion is given as:

$$\tau_P = I_P\,\ddot{\theta}_P + B_P\,\dot{\theta}_P + m_p g\,L_{GP}\,\theta_P \tag{14}$$

where τ_p is the torque applied by the FUM-Physio motor in CW direction, I_P is the arm inertia about the pivot point, m_p is the mass of the arm, L_{GP} is the distance from the center of gravity of the arm to the pivot point and θ_P is the arm angle measured in CW direction. τ_P and θ_P are illustrated in Figure 10. Note that the equation (14) is obtained for small angular displacement from the vertical equilibrium position, i.e. $\theta_p \cong 0$.

When the FUM-LSEA is installed, it applies forces along its longitudinal direction, producing an additional torque about the pivot point as given in equations (15) and (16):

$$\tau_P \cong I_P\,\ddot{\theta}_P + B_P\,\dot{\theta}_P + m_p g\,L_{GP}\,\theta_P - F_s d_1 \sin(\theta_{s0}) \tag{15}$$

$$\tau_P \cong I_P\,\ddot{\theta}_P + B_P\,\dot{\theta}_P + m_p g\,L_{GP}\,\theta_P - RF_s \tag{16}$$

where:

Figure 10 Kinematic parameters of compliantly actuated FUM-Physio

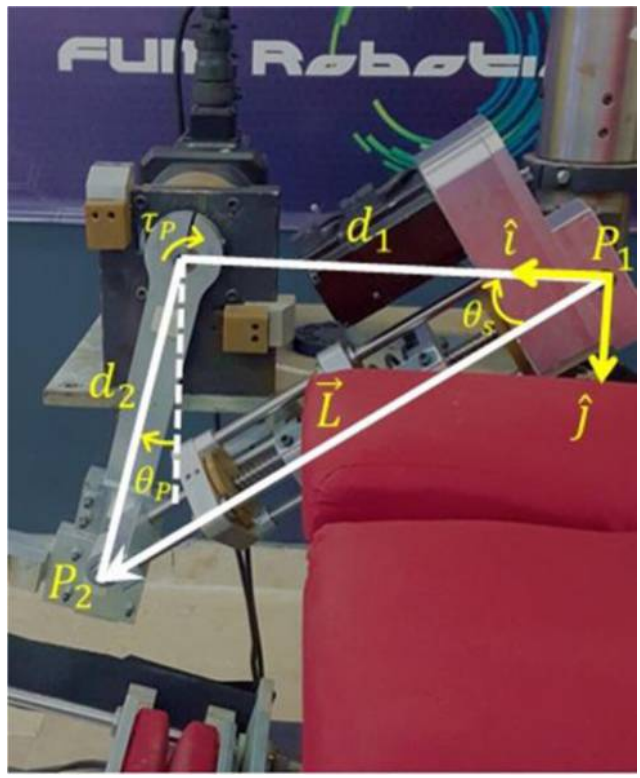

$$R = \frac{d_1 d_2}{\sqrt{d_1^2 + d_2^2}} \tag{17}$$

and θ_s is the SEA angle, formed between SEA longitudinal direction and the $\hat{\imath}$ vector, and θ_{s0} is the SEA angle for $\theta_P = 0$. F_s is the force applied from the FUM-LSEA to the arm and d_1 and d_2 are two constants that locate the position of the installation points of the FUM-LSEA on the base and the arm of the FUM-Physio. These points are denoted as P_1 and P_2 in Figure 10. F_s can be calculated from equation (7), remembering that x_h is the displacement of the output link of the SEA. According to Figure 10, x_h equals the displacement of the point P_2 along the longitudinal direction of the SEA which can be calculated as:

$$\begin{aligned}
\vec{L} &\cong (d_1 + d_2\theta_P)\hat{\imath} + d_2\hat{\jmath} \\
\vec{L}_0 &= d_1\hat{\imath} + d_2\hat{\jmath} \\
\hat{L}_0 &= \frac{d_1}{\sqrt{d_1^2 + d_2^2}}\,\hat{\imath} + \frac{d_2}{\sqrt{d_1^2 + d_2^2}}\,\hat{\jmath} \\
\overrightarrow{\Delta L} &= \vec{L} - \vec{L}_0 \cong d_2\theta_P\hat{\imath}
\end{aligned} \tag{18}$$

$$x_h \cong \overrightarrow{\Delta L} \cdot \hat{L}_0 \cong \frac{d_1 d_2}{\sqrt{d_1^2 + d_2^2}}\theta_P \cong R\theta_P \tag{19}$$

where $\hat{\imath}$ and $\hat{\jmath}$ are the unit vectors of the coordinate system, vector $\vec{L}$ extends from point P_1 to point P_2 and defines the

length of the FUM-LSEA, $\vec{L}_0$ equals $\vec{L}$ at $\theta_P = 0$ and $\hat{L}_0$ is a unit vector along the longitudinal direction of the FUM-LSEA at $\theta_P = 0$ (Figure 10).

Finally, the linearized equation of motion of the FUM-Physio coupled to the FUM-LSEA is obtained as:

$$\tau_P = I_P \ddot{\theta}_P + (B_P + R^2 B_s)\dot{\theta}_P + (m_P g L_{GP} + R^2 K_s)\theta_P - RB_s \dot{x}_m - RK_s x_m \quad (20)$$

Implementing the OFAC method, the position of the FUM-LSEA motor will be set as a function of displacement and velocity of the output link as given in equation (21):

$$x_m = \alpha x_h + \beta \dot{x}_h = \alpha R\theta_P + \beta R\dot{\theta}_P \quad (21)$$

Finally, the apparent IA of the assisted system can be calculated as given in equation (22) where, $K_P = m_P g L_{GP}$, $B_s' = R^2 B_s$ and $K_s' = R^2 K_s$:

$$\tau_P = I_t \ddot{\theta}_P + B_t \dot{\theta}_P + K_t \theta_P \quad \begin{cases} I_t = I_P - \beta B_s' \\ B_t = B_P - \beta K_s' - (\alpha - 1)B_s' \\ K_t = K_P - (\alpha - 1)K_s' \end{cases} \quad (22)$$

6.3 Experimentation

The OFAC control algorithm is implemented by using MATLAB/Simulink desktop real-time toolbox in a PC which communicates with motor drives through a TSP MDI motion control card made by tsPishro Company. Communication between PC and TSP MDI card is realized through an Ethernet connection.

6.3.1 First test

Installing the FUM-LSEA, the FUM-Physio can be considered as a 1-DOF SEA powered exoskeleton in which the servo motor acts as the knee joint and the robot arm resembles the assembly of the wearer's leg and the exoskeleton body. Therefore, this robot can be used for practical verification of the OFAC method by applying the following procedure. First, the FUM-LSEA is uninstalled and the FUM-Physio motor is controlled to move the arm in some specific angular trajectories. The required motor torques for running these trajectories are measured through CN5 analog monitor output of the motor drive. Next, the FUM-LSEA is installed on the robot and the OFAC method is implemented to control the position of the FUM-LSEA motor. Then, the torques required by the FUM-Physio motor for running the same trajectories are measured again. Finally, the lower torques of the second case will indicate the successful operation of the OFAC method. An overview of the control hardware is depicted in Figure 11.

Performing a combination of measurements and simple identification procedures, kinematic and dynamic parameters of the FUM-Physio and FUM-LSEA are roughly estimated as given in Table II.

Solving the constrained optimization of equation (13), maximum assistance ratio of $A(\omega_f) = 0.33$ is achieved, and optimal control parameters are obtained as $\alpha = 1.012$ and $\beta = 0.004$ for $\delta = 0.2$ and $\omega_f = 10\ [rad/s]$. Figure 12 compares the magnitude and phase diagrams of the IA of

Figure 11 Overview of the Control hardware for implementing the OFAC method on SEA powered FUM-Physio

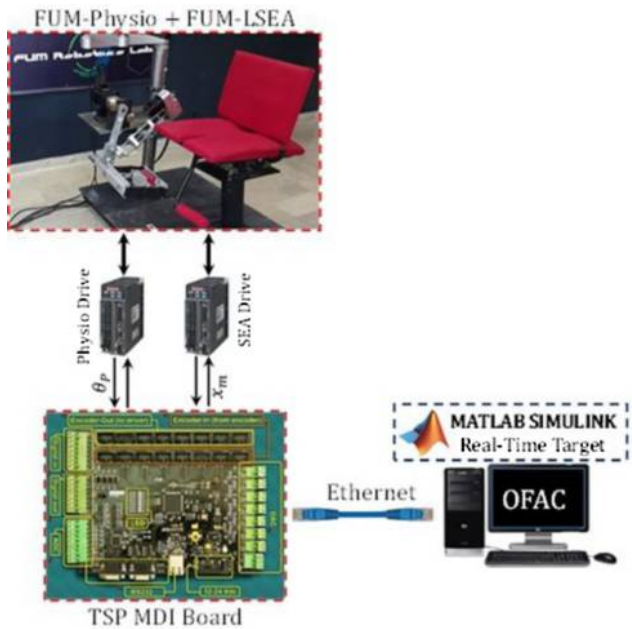

Table II Identified parameters of the FUM-Physio and FUM-LSEA

Parameter	Value
$I_P\ [kgm^2]$	0.53
$B_P\ [Nms/rad]$	3.31
$m_P g L_{GP}\ [Nm]$	12.61
$d_1\ [m]$	0.29
$d_2\ [m]$	0.23
$R\ [m]$	0.18
$K_s\ [kN/m]$	8.60
$B_s\ [Ns/m]$	2.56

the unassisted FUM-Physio with those of the optimally assisted robot. The point assistance ratio profile is also shown in Figure 12(b).

Figure 12 indicates that here again the maximum assistance occurs at damped natural frequency of the unassisted system, $\omega_d = 3.74\ [rad/s]$. It is also clear that the controller has a great phase shifting performance in the vicinity of this frequency. Moreover, Figure 12(c) clearly shows that the OFAC method has successfully met the comfort condition by keeping a low phase difference between the assisted and the unassisted stage.

As the first step of the experimental evaluation and before connecting the FUM-LSEA, two harmonic angle trajectories are applied to the FUM-Physio and the required torque trajectories are measured. The first trajectory, Path I, has amplitudes of 20 [°] and a frequency of 2 [*rad/s*]. The second trajectory, Path II, has amplitudes of 30 [°] and a frequency of 3 [*rad/s*]. Next, the FUM-LSEA is installed and the optimal OFAC algorithm is implemented. The same motions are applied to the robot and the required torque trajectories are measured again. Figure 13 compares the required torque

Figure 12 Performance of the OFAC method in the first experiment

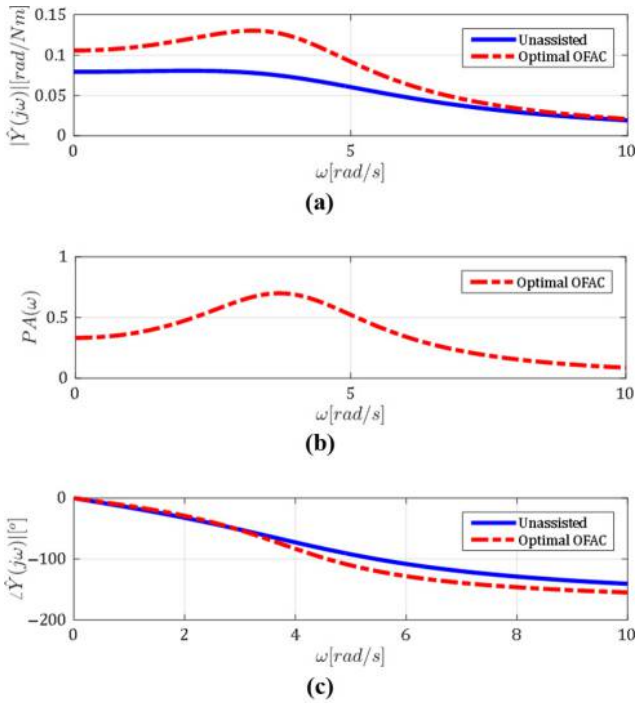

Notes: (a) Magnitude diagram; (b) point assistance profile; (c) phase diagram

Figure 13 Comparison of the required torque trajectories of the unassisted and the optimally assisted FUM-Physio

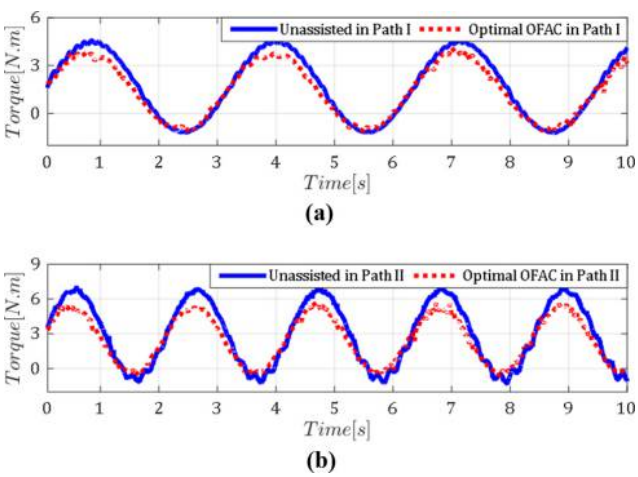

trajectories for the cases of the unassisted and the optimally assisted robot.

Figure 13 illustrates that, compared with the isolated robot, the assisted FUM-Physio requires lower external torques which in turn indicates effective performance of the OFAC method. The small phase difference between the unassisted and the optimally assisted system is also evident from Figure 13.

It is noteworthy that, the position of the actuator is defined by the OFAC method, as $x_m = \alpha R\theta_P + \beta R\dot{\theta}_P$, and applied through position mode of the FUM-LSEA motor drive. Rotation of the arm, θ_P, is measured via a feedback signal from the embedded encoder of the FUM-Physio motor while the angular velocity of the arm, $\dot{\theta}_P$, is estimated by using a high gain observer (HGO) whose general structure is given as (Vasiljevic and Khalil, 2006):

$$\begin{cases} \dot{\hat{x}}_1 = \hat{x}_2 + (\gamma/\varepsilon)(y - \hat{x}_1), \\ \dot{\hat{x}}_2 = (\gamma/\varepsilon^2)(y - \hat{x}_1), \\ y = x_1 = \theta_P \end{cases} \tag{23}$$

in which $y = x_1 = \theta_P$ is the measured link angle and $\hat{x}_2 = \hat{\dot{\theta}}_P$ is an estimation of the angular velocity. γ and ε are observer gains that determine its transient behavior and chosen as $\gamma = 10$ and $\varepsilon = 0.005$.

6.3.2 Second test

In the second test, a healthy human subject is placed on the FUM-Physio robot whose motor is set to apply no torques. The subject is asked to follow a given trajectory, displayed on the monitor, while the sEMG signals of the knee muscles are measured. As shown in Figure 14, the three Vastus Lateralis, Rectus Femoris and Vastus Medialis muscles are, respectively, measured through first, second and third sEMG channels, while the reference electrodes are placed on the patella bone. The subject's skin is carefully shaved and cleaned with alcohol to strengthen the sEMG signals. It should be noted that, the sEMG signals are merely used for monitoring the loads on the knee muscles of the operator. Obviously, these signals do not take part in the implementation of the OFAC method and used only to display the ability of the proposed method in reducing the loads on real human operators.

Figure 14 The subject on FUM-Physio and the location of sEMG electrodes

The amplified sEMG signals are filtered using a normalized Butterworth filter with a passband frequency of 10 to 500 Hz. The signals are then rectified and their root-mean-square envelopes, $E(n)$, are calculated by considering a moving window of a width of $N = 100$ samples as:

$$E(n) = \sqrt{\frac{1}{N}\sum_{i=0}^{N-1} E_{fr}^2(n-i)} \quad (24)$$

where, E_{fr} represents the filtered rectified version of the raw sEMG signals. It is well known that the envelopes of the sEMG signals reflect the forces applied by the corresponding knee muscles.

This test is also performed in two steps. In the first step, the FUM-LSEA is unmounted from the FUM-Physio and the subject is asked to follow the desired angular trajectory which is shown on the monitor along with the actual angular position of the subject's knee. The sEMG signals of the aforementioned knee muscles are recorded and their envelopes are extracted. In the second step, the FUM-LSEA is connected and the optimal OFAC algorithm is implemented. The subject is asked to follow the same angular trajectory and the sEMG signals are recorded again. The reduced amplitude of the sEMG envelopes will indicate the reduction in the muscles' efforts as well as the successful performance of the OFAC method. Note that in both steps, before recording the EMG signals, the subject is allowed to repeat the motions for several times to get familiar with the trajectories and to minimize the tracking error.

A rigid connection is assumed between the subject's leg and the robot arm. Therefore, they can be considered as a single link and the same modeling of the Section 6.2 applies here. However, in this case, the dynamic parameters of the subject's leg are added to those of the robot arm. Table III gives a rough estimation of the dynamic parameters of the arm and leg assembly, obtained from a set of measurements and identification procedures.

Using the values of Table III and solving equation (13) for $\delta = 0.2$ and $\omega_f = 10\ [rad/s]$, the optimal assistance ratio of $\mathcal{A}(\omega_f) = 0.33$ is obtained for $\alpha = 1.02$ and $\beta = 0.006$. Figure 15 depicts the magnitude and phase diagrams of the unassisted and the optimally assisted systems and the point assistance profile provided by the optimal controller. Note that the maximum point assistance is obtained at damped natural frequency of the unassisted system, $\omega_d = 4.51\ [rad/s]$.

The desired knee angular trajectory is considered as a harmonic motion with an amplitude of 30 [^{o}] and a frequency of 3 [rad/s] and the filtered sEMG signals are provided in Figure 16. The sEMG envelopes for the unassisted and optimally assisted motions of the first and second steps of the test are compared in Figure 17. Note that only the parts of sEMG envelopes between 28 and 44 s are provided in Figure 17 in order to facilitate the comparison.

Figure 17 shows that the amplitudes of the sEMG envelopes of all the three knee muscles are effectively reduced during the assisted motion of the second step. This in turn indicates the reduced burden on the knee joint and verifies the successful performance of the OFAC method in the case of real human operators. In addition to assisting the exoskeleton users to move easier, reducing the loads on the patients' muscles helps them in extending the motion range of the affected limb and expediting the physiotherapy process.

It is noteworthy that the HGO of equation (23) with the same parameters values is also used in the second test for estimating the velocity signals from the measured position signal.

Table III Identified parameters of the assembly of the FUM-Physio arm and the subject's leg

Parameter	Value
$I_P\ [kgm^2]$	0.81
$B_P\ [Nms/rad]$	4.72
$m_P g L_{GP}\ [Nm]$	23.35
$d_1\ [m]$	0.29
$d_2\ [m]$	0.23
$R\ [m]$	0.18

Figure 15 Performance of the OFAC method in the second experiment

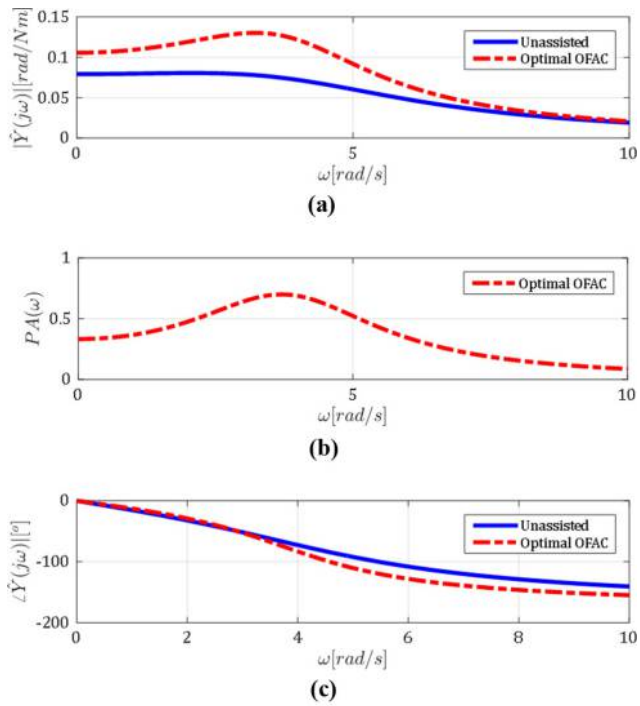

Notes: (a) Magnitude diagram; (b) point assistance profile; (c) phase diagram

7. Conclusions

The main contribution of this paper is to propose a novel output feedback assistive controller for single DOF compliantly actuated systems. The proposed OFAC method increases apparent IA of the assisted system without any information about interaction forces or intended motions of the system. Therefore, there will be no need for extra sensors such as load cells, EMG sensors and accelerometers, which have some well-known problems in practical applications.

Figure 16 Filtered sEMG signals for the three channels during the unassisted and optimally assisted motions

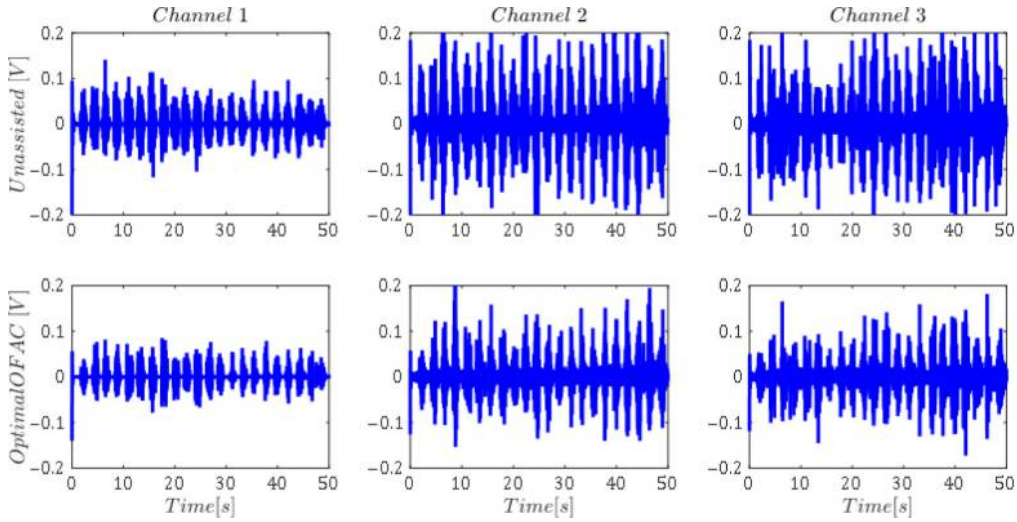

Figure 17 Comparing the amplitudes of the sEMG envelopes for the unassisted and optimally assisted motions

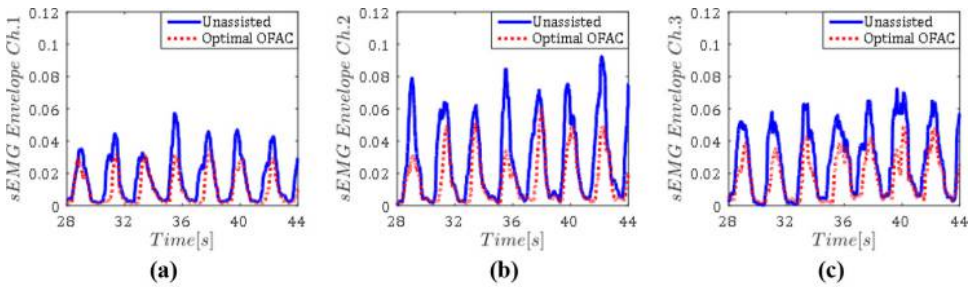

Notes: (a) 1st channel for Vastus Lateralis; (b) 2nd channel for Rectus Femoris; (c) 3rd channel for Vastus Medialis

The assistance ratio is used as the performance criterion for the proposed controller. A new comfort measure is defined in terms of the phase difference between the assisted and the unassisted system. This measure acts as a constraint to maximization of the assistance ratio. Stability and coupled stability conditions of the assisted system are derived and applied as additional constraints on the optimization problem. Finally, a constrained optimization problem is defined to find optimal controller coefficients.

Performance of the proposed OFAC method is compared to IA shaping algorithm (Nagarajan *et al.*, 2016) through some simulations. Simulation results indicate that the proposed OFAC method can provide a comparable performance with fewer sensors and less number of adjustable control coefficients. Moreover, the results show that the OFAC method completely outperforms the IA shaping algorithm (Nagarajan *et al.*, 2016), in frequencies close to the natural frequency of the simulated system.

The OFAC method is further evaluated in practical conditions by using the 1-DOF lower limb exoskeleton, FUM-Physio, as a test bed for performing the experiments. Two separate tests are designed and performed for practical evaluation of the OFAC method. Even though only rough estimations of the system parameters are used, the experimental results clearly show the effective performance of the proposed method. This achievement is the result of the simple model-free structure of the OFAC method. The system will be more or less assisted as long as the control coefficients are chosen within the permissible region. In fact, the parameter values only affect the boundaries of the permissible region and the optimality of applied controller. The results also reveal that the OFAC method can be successfully implemented by using only position sensors and estimating the velocity feedback through a HGO.

It is well known that defining the exact values of dynamic parameters of human limbs is not an easy task, and these values may even change during different tasks. Moreover, the values of system parameters are roughly estimated in both tests. Therefore, successful operation of the OFAC method in the presented tests, specifically in connection with a real human operator, somehow indicates the robustness of the proposed method.

Eliminating the need for extra sensors, besides other desirable features like simple model-free structure, enables the use of the proposed controller as a good choice in the assistive control of dynamical systems, specifically exoskeleton robots. Future works may focus on extending the OFAC method to multi-DOF exoskeletons and evaluating the robustness of the proposed algorithm against uncertainties and parameter changes.

References

Aguirre-Ollinger, G., Colgate, J.E., Peshkin, M. and Goswami, A. (2007), "Active-impedance control of a lower-limb assistive exoskeleton", *IEEE 10th International Conference on Rehabilitation Robotics*, *Noordwijk*, *13-15 June*, pp. 188-195.

Aguirre-Ollinger, G., Colgate, J.E., Peshkin, M.A. and Goswami, A. (2011), "Design of an active one-degree-of-freedom lower-limb exoskeleton with inertia compensation", *The International Journal of Robotics Research*, Vol. 30 No. 4, pp. 486-499.

Aguirre-Ollinger, G., Colgate, J.E., Peshkin, M. and Goswami, A. (2012), "Inertia compensation control of a one-degree-of-freedom exoskeleton for lower-limb assistance: initial experiments", *IEEE Transactions on Neural Systems and Rehabilitation Engineering*, Vol. 20 No. 1, pp. 68-77.

Amini, H., Rezaei, S.M., Sarhan, A.A., Akbari, J. and Mardi, N.A. (2015), "Transparency improvement by external force estimation in a time-delayed nonlinear bilateral Teleoperation system", *Journal of Dynamic Systems, Measurement, and Control*, Vol. 137 No. 5, p. 051013.

Bogue, R. (2009), "Exoskeletons and robotic prosthetics: a review of recent developments", *Industrial Robot: An International Journal*, Vol. 36 No. 5, pp. 421-427.

Cestari, M., Sanz-Merodio, D., Arevalo, J.C. and Garcia, E. (2014), "ARES, a variable stiffness actuator with embedded force sensor for the ATLAS exoskeleton", *Industrial Robot: An International Journal*, Vol. 41 No. 6, pp. 518-526.

Cheng, H.S., Ju, M.S. and Lin, C.C.K. (2003), "Improving elbow torque output of stroke patients with assistive torque controlled by EMG signals", *Journal of Biomechanical Engineering*, Vol. 125 No. 6, pp. 881-886.

Colgate, J.E. (1988), "The control of dynamically interacting systems", *Doctoral Dissertation*, MA Institute of Technology, MA.

Esquenazi, A., Talaty, M., Packel, A. and Saulino, M. (2012), "The ReWalk powered exoskeleton to restore ambulatory function to individuals with thoracic-level motor-complete spinal cord injury", *American Journal of Physical Medicine & Rehabilitation*, Vol. 91 No. 11, pp. 911-921.

Fite, K.B., Shao, L. and Goldfarb, M. (2004), "Loop shaping for transparency and stability robustness in bilateral telemanipulation", *IEEE Transactions on Robotics and Automation*, Vol. 20 No. 3, pp. 620-624.

Focchi, M., Medrano-Cerda, G.A., Boaventura, T., Frigerio, M., Semini, C., Buchli, J. and Caldwell, D.G. (2016), "Robot impedance control and passivity analysis with inner torque and velocity feedback loops", *Control Theory and Technology*, Vol. 14 No. 2, pp. 97-112.

Haddadi, A. and Hashtrudi-Zaad, K. (2010), "Bounded-impedance absolute stability of bilateral teleoperation control systems", *IEEE Transactions on Haptics*, Vol. 3 No. 1, pp. 15-27.

Haddadi, A., Razi, K. and Hashtrudi-Zaad, K. (2015), "Operator dynamics consideration for less conservative coupled stability condition in bilateral teleoperation", *IEEE/ASME Transactions on Mechatronics*, Vol. 20 No. 5, pp. 2463-2475.

Hogan, N. (1989), "Controlling impedance at the man/machine interface", *Proceedings of IEEE International Conference on Robotics and Automation*, *Scottsdale, AZ*, *14-19 May*, pp. 1626-1631.

Hussain, S., Xie, S.Q. and Jamwal, P.K. (2013), "Adaptive impedance control of a robotic orthosis for gait rehabilitation", *Cybernetics, IEEE Transactions on*, Vol. 43 No. 3, pp. 1025-1034.

Kamali, K., Akbari, A.A. and Akbarzadeh, A. (2016), "Trajectory generation and control of a knee exoskeleton based on dynamic movement primitives for sit-to-stand assistance", *Advanced Robotics*, Vol. 30 No. 13, pp. 846-860.

Karavas, N., Ajoudani, A., Tsagarakis, N., Saglia, J., Bicchi, A. and Caldwell, D. (2015), "Tele-impedance based assistive control for a compliant knee exoskeleton", *Robotics and Autonomous Systems*, Vol. 73 No. 1, pp. 78-90.

Kawamoto, H. and Sankai, Y. (2002), "Power assist system HAL-3 for gait disorder person", in Miesenberger, K., Klaus, J. and Zagler, W. (Eds), *Computers Helping People with Special Needs*, Springer, Berlin, Heidelberg, pp. 196-203.

Kazerooni, H. and Steger, R. (2006), "The Berkeley lower extremity exoskeleton", *Journal of Dynamic Systems, Measurement and Control*, Vol. 128 No. 1, pp. 14-25.

Kazerooni, H., Steger, R. and Huang, L. (2006), "Hybrid control of the Berkeley lower extremity exoskeleton (BLEEX)", *The International Journal of Robotics Research*, Vol. 25 Nos 5/6, pp. 561-573.

Kiguchi, K., Tanaka, T. and Fukuda, T. (2004), "Neuro-fuzzy control of a robotic exoskeleton with EMG signals", *IEEE Transactions on Fuzzy Systems*, Vol. 12 No. 4, pp. 481-490.

Kiguchi, K., Kariya, S., Watanabe, K., Izumi, K. and Fukuda, T. (2001), "An exoskeletal robot for human elbow motion support-sensor fusion, adaptation, and control", *IEEE Transactions on Systems, Man, and Cybernetics, Part B: Cybernetics*, Vol. 31 No. 3, pp. 353-361.

Kopp, C. (2011), "Exoskeletons for warriors of the future", *Defense To-day*, Vol. 9 No. 2, pp. 38-40, available at: http://arrow.monash.edu.au/hdl/1959.1/817161

Kuo, A.D. (2001), "A simple model of bipedal walking predicts the preferred speed–step length relationship", *Journal of Biomechanical Engineering*, Vol. 123 No. 3, pp. 264-269.

Lawrence, D.A. (1993), "Stability and transparency in bilateral teleoperation", *IEEE Transactions on Robotics and Automation*, Vol. 9 No. 5, pp. 624-637.

Lawrence, D.A. and Chapel, J.D. (1994), "Performance trade-offs for hand controller design", *Proceedings of IEEE International Conference on Robotics and Automation*, *San Diego, CA*, *8 May*, pp. 3211-3216.

Lee, D. and Spong, M.W. (2006), "Passive bilateral teleoperation with constant time delay", *IEEE Transactions on Robotics*, Vol. 22 No. 2, pp. 269-281.

Lee, S. and Sankai, Y. (2002a), "Power assist control for walking aid with HAL-3 based on EMG and impedance adjustment around knee joint", *IEEE/RSJ International Conference on Intelligent Robots and Systems*, *EPFL*, *30 September-4 October*, Vol. 2, pp. 1499-1504.

Lee, S. and Sankai, Y. (2002b), "Power assist control for leg with HAL-3 based on virtual torque and impedance adjustment", *IEEE International Conference on Systems, Man and Cybernetics, Hammamet, 6-9 October*, Vol. 4.

Morbi, A., Ahmadi, M., Chan, A.D. and Langlois, R. (2014), "Stability-guaranteed assist-as-needed controller for powered orthoses", *IEEE Transactions on Control Systems Technology*, Vol. 22 No. 2, pp. 745-752.

Mosher, R.S. (1967), "Handyman to hardiman", SAE Technical Paper, No. 670088, 1 February.

Nagarajan, U., Aguirre-Ollinger, G. and Goswami, A. (2016), "Integral admittance shaping: a unified framework for active exoskeleton control", *Robotics and Autonomous Systems*, Vol. 75, pp. 310-324.

Niemeyer, G. and Slotine, J.J. (1991), "Stable adaptive teleoperation", *IEEE Journal of Oceanic Engineering*, Vol. 16 No. 1, pp. 152-162.

Pratt, J., Krupp, B. and Morse, C. (2002), "Series elastic actuators for high fidelity force control", *Industrial Robot: An International Journal*, Vol. 29 No. 3, pp. 234-241.

Pratt, J.E., Krupp, B.T., Morse, C.J. and Collins, S.H. (2004), "The RoboKnee: an exoskeleton for enhancing strength and endurance during walking", *Proceedings of the IEEE International Conference on Robotics & Automation, ICRA '04, New Orleans, LA*, 26 April-1 May, pp. 2430-2435.

Ronsse, R., Lenzi, T., Vitiello, N., Koopman, B., van Asseldonk, E., De Rossi, S.M.M., van den Kieboom, J., van der Kooij, H., Carrozza, M.C. and Ijspeert, A.J. (2011), "Oscillator-based assistance of cyclical movements: model-based and model-free approaches", *Medical and Biological Engineering and Computing*, Vol. 49 No. 10, pp. 1173-1185.

Rosen, J., Brand, M., Fuchs, M.B. and Arcan, M. (2001), "A myosignal-based powered exoskeleton system", *IEEE Transactions on Systems and Humans*, Vol. 31 No. 3, pp. 210-222.

Ryu, J.H., Kwon, D.S. and Hannaford, B. (2004), "Stability guaranteed control: time domain passivity approach", *IEEE Transactions on Control Systems Technology*, Vol. 12 No. 6, pp. 860-868.

Sankai, Y. (2010), "HAL: Hybrid assistive limb based on cybernics", in Kaneko, M. and Nakamura, Y. (Eds), *Robotics Research*, Springer, Berlin, Heidelberg, pp. 25-34.

Sirouspour, S. and Shahdi, A. (2006), "Model predictive control for transparent teleoperation under communication time delay", *IEEE Transactions on Robotics*, Vol. 22 No. 6, pp. 1131-1145.

Tang, A. and Cao, Q. (2012), "Motion control of walking assistant robot based on comfort", *Industrial Robot: An International Journal*, Vol. 39 No. 6, pp. 564-579.

Uemura, M., Kanaoka, K. and Kawamura, S. (2006), "Power assist systems based on resonance of passive elements", *IEEE/RSJ International Conference on Intelligent Robots and Systems, Beijing, 9-15 October*, pp. 4316-4321.

Unluhisarcikli, O., Pietrusinski, M., Weinberg, B., Bonato, P. and Mavroidis, C. (2011), "Design and control of a robotic lower extremity exoskeleton for gait rehabilitation", *IEEE/RSJ International Conference on Intelligent Robots and Systems, San Francisco, CA, 25-30 September*, pp. 4893-4898.

Vallery, H., Veneman, J., Asseldonk, E.V., Ekkelenkamp, R., Buss, M. and Kooij, H.V.D. (2008), "Compliant actuation of rehabilitation robots", *Robotics & Automation Magazine, IEEE*, Vol. 15 No. 3, pp. 60-69.

Vander Poorten, E.B., Yokokohji, Y. and Yoshikawa, T. (2006), "Stability analysis and robust control for fixed-scale teleoperation", *Advanced Robotics*, Vol. 20 No. 6, pp. 681-706.

Vanderborght, B., Albu-Schäffer, A., Bicchi, A., Burdet, E., Caldwell, D.G., Carloni, R., Catalano, M., Eiberger, O., Friedl, W., Ganesh, G. and Garabini, M. (2013), "Variable impedance actuators: a review", *Robotics and Autonomous Systems*, Vol. 61 No. 12, pp. 1601-1614.

Vasiljevic, L.K. and Khalil, H.K. (2006), "Differentiation with high-gain observers the presence of measurement noise", *IEEE Conference on Decision and Control, San Diego, CA, 13-15 December*, pp. 4717-4722.

Veneman, J.F., Kruidhof, R., Hekman, E.E., Ekkelenkamp, R., Van Asseldonk, E.H. and Van Der Kooij, H. (2007), "Design and evaluation of the LOPES exoskeleton robot for interactive gait rehabilitation", *Neural Systems and Rehabilitation Engineering, IEEE Transactions on*, Vol. 15 No. 3, pp. 379-386.

Vukobratovic, M.K. (2007), "When were active exoskeletons actually born?", *International Journal of Humanoid Robotics*, Vol. 4 No. 3, pp. 459-486.

Yan, T., Cempini, M., Oddo, C.M. and Vitiello, N. (2015), "Review of assistive strategies in powered lower-limb orthoses and exoskeletons", *Robotics and Autonomous Systems*, Vol. 64, pp. 120-136.

Corresponding author

Alireza Akbarzadeh can be contacted at: Ali_Akbarzadeh@um.ac.ir